

# FOCUSING SINGULARITY IN A DERIVATIVE NONLINEAR SCHRÖDINGER EQUATION

XIAO LIU, GIDEON SIMPSON, AND CATHERINE SULEM

ABSTRACT. We present a numerical study of a derivative nonlinear Schrödinger equation with a general power nonlinearity,  $|\psi|^{2\sigma} \psi_x$ . In the  $L^2$ -supercritical regime,  $\sigma > 1$ , our simulations indicate that there is a finite time singularity. We obtain a precise description of the local structure of the solution in terms of blowup rate and asymptotic profile, in a form similar to that of the nonlinear Schrödinger equation with supercritical power law nonlinearity.

## 1. INTRODUCTION

We consider the derivative nonlinear Schrödinger (DNLS) equation

$$(1.1) \quad i\partial_t \Psi + \Psi_{xx} + i(|\Psi|^2 \Psi)_x = 0, \quad x \in \mathbb{R}, \quad t \in \mathbb{R}$$

with initial condition  $\Psi(x, 0) = \Psi_0(x)$ . Under a long wavelength approximation, this nonlinear dispersive wave equation is a model for Alfvén waves in plasma physics, [17, 19, 21]. Using a Gauge transformation,

$$(1.2) \quad \psi = \Psi(x) \exp \left\{ \frac{1}{2} \int_{-\infty}^x |\Psi(\eta)|^2 d\eta \right\},$$

(1.1) takes the form

$$(1.3) \quad i\partial_t \psi + \psi_{xx} + i|\psi|^2 \psi_x = 0, \quad x \in \mathbb{R}, \quad t \in \mathbb{R}.$$

This equation appeared in studies of ultrashort optical pulses, [1, 18]. The latter equation admits a Hamiltonian form

$$(1.4) \quad \partial_t \psi = -i \frac{\delta E}{\delta \psi}$$

---

*Date:* June 23, 2021.

*1991 Mathematics Subject Classification.* 35Q55, 37K40, 35Q51, 65M60.

*Key words and phrases.* Derivative Nonlinear Schrödinger Equation, Singular Solutions, Rate of Blow-up, Dynamical Rescaling.

G.S. was supported by NSERC. His contribution to this work was completed under the NSF PIRE grant OISE-0967140 and the DOE grant DE-SC0002085.

C.S. is partially supported by NSERC through grant number 46179-11.

with the Hamiltonian

$$(1.5) \quad E = \frac{1}{2} \int_{-\infty}^{\infty} |\psi_x|^2 dx + \frac{1}{4} \Im \int_{-\infty}^{\infty} |\psi|^2 \bar{\psi} \psi_x dx.$$

The well-posedness of (1.1) has been studied by many authors. One of the earliest results is due to Tsutsumi and Fukuda, who proved local well-posedness on both  $\mathbb{R}$  and  $\mathbb{T}$  in the Sobolev space  $H^s$ , provided  $s > 3/2$  and the data is sufficiently small, [22]. This was subsequently refined by Hayashi and Ozawa, who found that for initial conditions satisfying

$$(1.6) \quad \|u_0\|_{L^2} < \sqrt{2\pi},$$

the solution was global in  $H^s$  for  $s \in \mathbb{N}$ , [6]. More recently, the global in time result for data satisfying (1.6) was extended to all  $H^s$  spaces with  $s > 1/2$ , [2].

Local well posedness has also been studied with additive terms, [3], and with more general nonlinearities, [10,14]. However, an outstanding problem for DNLS is to determine the fate of large data, violating (1.6). At present, there is neither a result on global well posedness, nor is there a known finite time singularity.

In this paper, we consider a generalized derivative nonlinear Schrödinger (gDNLS) equation of the form ( $\sigma \geq 1$ )

$$(1.7) \quad i\partial_t \psi + \psi_{xx} + i|\psi|^{2\sigma} \psi_x = 0, \quad x \in \mathbb{R}, \quad t \in \mathbb{R}.$$

It also has a Hamiltonian structure with generalized energy:

$$(1.8) \quad E = \frac{1}{2} \int_{-\infty}^{\infty} |\psi_x|^2 dx + \frac{1}{2(\sigma+1)} \Im \int_{-\infty}^{\infty} |\psi|^{2\sigma} \bar{\psi} \psi_x dx,$$

along with the mass and momentum invariants:

$$(1.9) \quad M = \frac{1}{2} \int_{-\infty}^{\infty} |\psi|^2 dx,$$

$$(1.10) \quad P = -\frac{1}{2} \Im \int_{-\infty}^{\infty} \bar{\psi} \psi_x dx.$$

For  $\sigma > 5/2$ , the local well-posedness for (1.7) is proved for initial data in  $H^{1/2}$  intersected with an appropriate Strichartz space, [5].

For all values of  $\sigma$ , we have the scaling property that if  $\psi(x, t)$  is a solution of (1.7), then so is

$$(1.11) \quad \psi_\lambda(x, t) = \lambda^{-\frac{1}{2\sigma}} \psi(\lambda^{-1}x, \lambda^{-2}t).$$

Hence, (1.7) is  $L^2$ -critical for  $\sigma = 1$  and  $L^2$ -supercritical for  $\sigma > 1$ . It is well known that the  $L^2$ -supercritical NLS equation with power law nonlinearity has finite time singularities for sufficiently large data. The

goal of this work is to explore the potential for collapse in (1.7) when  $\sigma > 1$ .

Our simulations and asymptotics indicate that there is collapse, and we give an accurate description of the nature of the focusing singularity with generic “large” data. This is done using the dynamic rescaling method, which was introduced to study the local structure of NLS singularities, [16, 21]. The idea behind dynamic rescaling is to introduce an adaptive grid through a nonlinear change of variables based on the scaling invariance of the equation. Up to a rescaling, we observe numerically for  $\sigma > 1$ , the solution blows up locally like

$$(1.12) \quad \psi(x, t) \sim \left( \frac{1}{2\alpha(t^* - t)} \right)^{\frac{1}{4\sigma}} Q \left( \frac{x - x^*}{\sqrt{2\alpha(t^* - t)}} + \frac{\beta}{\alpha} \right) e^{i(\theta + \frac{1}{2\alpha} \ln \frac{t^*}{t^* - t})},$$

where  $t^*$  is the singularity time and  $x^*$  is the position of  $\max_x |\psi(x, t^*)|$ . The function  $Q(\xi)$  is a complex-valued solution of the equation

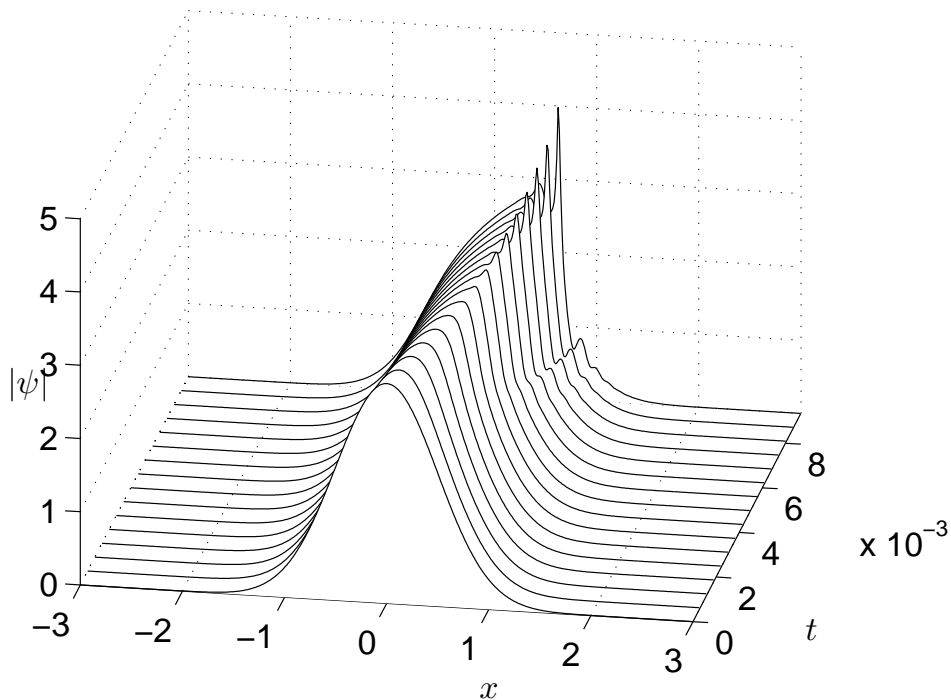
$$(1.13) \quad Q_{\xi\xi} - Q + i\alpha\left(\frac{1}{2\sigma}Q + \xi Q_\xi\right) - i\beta Q_\xi + i|Q|^{2\sigma}Q_\xi = 0,$$

with amplitude that decays monotonically as  $\xi \rightarrow \pm\infty$ . The coefficients  $\alpha$  and  $\beta$  are real numbers, and our simulations show that they depend on  $\sigma$  but not on the initial condition. We also observe that  $\alpha$  decreases monotonically as  $\sigma \rightarrow 1$ , while  $\beta$  first decreases then increases (Figure 15). This observed blowup is analogous to that of NLS with supercritical power nonlinearity in terms of the blowup speed and asymptotic profile, [16].

Our paper is organized as follows. In section 2, we consider gDNLS with quintic nonlinearity ( $\sigma = 2$ ). We first present a direct numerical simulation that suggests there is, indeed, a finite time singularity. We then refine our study by introducing the dynamic rescaling method. Section 3 shows our results for  $\sigma \in (1, 2)$ . In the Section 4, we discuss the asymptotic profile of gDNLS. We discuss our results in Section 5, and their implications for blowup in DNLS. Details of our numerical methods are described in the Appendix.

## 2. gDNLS WITH QUINTIC NONLINEARITY

We first performed a direct numerical integration of the the gDNLS equation with quintic nonlinearity ( $\sigma = 2$ ) and initial condition  $\psi_0 = 3e^{-2x^2}$ . We integrated the equation using a pseudo-spectral method with an exponential time-differencing fourth-order Runge-Kutta algorithm (ETDRK4), augmenting it with the numerical stabilization scheme presented in [8] to better resolve small wave numbers. The computation was performed on the interval  $[-8, 8)$ , with  $2^{12}$  grid points and a time step on the order of  $10^{-6}$ . Figure 1 shows that the wave first

FIGURE 1.  $|\psi(x, t)|$  versus  $x$  and  $t$ .

moves rightward and then begins to separate. Gradually, the leading edge of one wave sharpens and grows in time. The norms  $\|\psi_x(\cdot, t)\|_{L^2}$  and  $\|\psi_{xx}(\cdot, t)\|_{L^2}$  grow substantially during the lifetime of the simulation. The norm  $\|\psi_x(\cdot, t)\|_{L^2}$  increases from 4 to about 18 while  $\|\psi_{xx}(\cdot, t)\|_{L^2}$  increases from about 10 to 1720. This growth in norms is a first indication of collapse. In contrast, the  $L^\infty$  norm has only increased from 3 to 4.07. As a measure of the precision of the simulation, the energy remains equal to 7.976, with three digits of precision, up to time  $t = 0.009$ .

**2.1. Dynamical Rescaling Formulation.** To gain additional detail of the blowup, we employ the dynamic rescaling method. Based on the scaling invariance of the equation (1.11), we define the new variables: (2.1)

$$\psi(x, t) = L^{-\frac{1}{2\sigma}}(t)u(\xi, \tau), \quad \xi = \frac{x - x_0(t)}{L(t)} \quad \text{and} \quad \tau = \int_0^t \frac{ds}{L^2(s)},$$

where  $L(t)$  is a length scale parameter chosen such that a certain norm of the solution remains bounded for all  $\tau$ . The parameter  $x_0$  will be chosen to follow the transport of the solution. Substituting the change

of variables into (1.7) gives

$$(2.2) \quad \begin{aligned} iu_\tau + u_{\xi\xi} + ia(\tau)\left(\frac{1}{2\sigma}u + \xi u_\xi\right) - ib(\tau)u_\xi + i|u|^{2\sigma}u_\xi &= 0, \\ u(\xi, 0) &= \psi(x, 0), \end{aligned}$$

where

$$(2.3a) \quad a(\tau) = -L(t)\dot{L}(t) = -\frac{d \ln L}{d\tau},$$

$$(2.3b) \quad b(\tau) = L(t)\frac{dx_0}{dt}.$$

There are several possibilities for the choice of  $L(t)$ . We define  $L(t)$  such that  $\|u_\xi(\cdot, \tau)\|_{L^2}$  remains constant. From (2.1),

$$\|\psi_x\|_{L^{2p}} = L^{-\frac{1}{q}}\|u_\xi\|_{L^{2p}}, \quad q = \left(1 + \frac{1}{2}\left(\frac{1}{\sigma} - \frac{1}{p}\right)\right)^{-1},$$

and

$$L(t) = \|u_\xi(\cdot, 0)\|_{L^{2p}}^q \|\psi_x(\cdot, t)\|_{L^{2p}}^{-q},$$

leading to an integral expression for the function  $a(\tau)$  defined in (2.3a):

$$(2.4) \quad a(\tau) = -q\|u_\xi(\cdot, 0)\|_{L^{2p}}^{-2p} \int \Re\left\{(\bar{u}_\xi^p u_\xi^{p-1})_\xi (iu_{\xi\xi} - |u|^{2\sigma}u_\xi)\right\} d\xi,$$

Ideally, we would like to choose  $x_0(t)$  to follow the highest maximum of the amplitude of the solution. After several attempts, we found that choosing

$$(2.5) \quad x_0 = \frac{\int x|\psi_x|^{2p}dx}{\int |\psi_x|^{2p}dx}$$

follows the maximum of the amplitude in a satisfactory way. The coefficient  $b$  takes the form

$$(2.6) \quad b(\tau) = 2p \frac{\int \Re\left\{(\xi|u_{\xi\xi}|^{2p-2}\bar{u}_{\xi\xi})_{\xi\xi}(iu_{\xi\xi} - |u|^{2\sigma}u_\xi)\right\}d\xi}{\int |u_{\xi\xi}|^{2p}d\xi}.$$

In summary, we now have a system of evolution equations for the rescaled solution  $u$ :

$$(2.7a) \quad u_\tau = iu_{\xi\xi} - a(\tau)\left(\frac{1}{2\sigma}u + \xi u_\xi\right) + b(\tau)u_\xi - |u|^{2\sigma}u_\xi$$

$$(2.7b) \quad a(\tau) = -q\|u_\xi(0)\|_{L^{2p}}^{-2p} \int \Re\left\{(\bar{u}_\xi^p u_\xi^{p-1})_\xi (iu_{\xi\xi} - |u|^{2\sigma}u_\xi)\right\} d\xi,$$

$$(2.7c) \quad b(\tau) = 2p \frac{\int \Re\left\{(\xi|u_{\xi\xi}|^{2p-2}\bar{u}_{\xi\xi})_{\xi\xi}(iu_{\xi\xi} - |u|^{2\sigma}u_\xi)\right\}d\xi}{\int |u_{\xi\xi}|^{2p}d\xi}.$$

where  $p \in \mathbb{N}$  and  $q = \left(1 + \frac{1}{2}\left(\frac{1}{\sigma} - \frac{1}{p}\right)\right)^{-1}$ . The scaling factor  $L(\tau)$  is computed by integration of (2.3a).

We expect  $u(\xi, \tau)$  to be defined for all  $\tau$  and that  $L(\tau) \rightarrow 0$  fast enough so that  $\tau \rightarrow \infty$  as  $t \rightarrow t^*$ . The behavior of  $a(\tau)$  and  $u(\xi, \tau)$  for large  $\tau$  will give us information on the scaling factor  $L(\tau)$  and the limiting profile. Under this rescaling, the invariants (1.8), (1.9) and (1.10) become

$$(2.8a) \quad E(\psi(t)) = E(\psi(0)) = L(t)^{-\frac{1}{\sigma}-1} E(u(\tau)),$$

$$(2.8b) \quad M(\psi(t)) = M(\psi(0)) = L(t)^{-\frac{1}{\sigma}+1} M(u(\tau)),$$

$$(2.8c) \quad P(\psi(t)) = P(\psi(0)) = L(t)^{-\frac{1}{\sigma}} P(u(\tau)).$$

These relations allow us to compute  $L(t)$  in different ways and check the consistency of our calculations.

**2.2. Singularity Formation.** Integrating (2.2) using the ETDRK4 algorithm, we present our results for two families of initial conditions:

$$(2.9) \quad \psi_0(x) = A_0 e^{-2x^2} \quad (\text{Gaussian})$$

and

$$(2.10) \quad \psi_0(x) = \frac{A_0}{1 + 9x^2} \quad (\text{Lorentzian}).$$

with various values of the amplitude coefficient  $A_0$ . We observed that for both families, the corresponding solutions present similar local structure near the blowup time.

In these simulations, there are typically  $2^{18}$  points in the domain  $[-l, l]$  with  $l = 1024$ . While the exponential time differencing removes the stiffness associated with the second derivative term, the advective coefficient,

$$(a\xi - b + |u|^{2\sigma})u_\xi,$$

constrains our time step through a CFL condition. Near the origin, where  $u$ , initially, can have an amplitude as large as  $A_0 = 4$ , we have a coefficient for the quintic case that can be  $\sim 100$ . Far from the origin,  $a\xi$  is the dominant term, and this coefficient can be  $\sim 1000$ . Consequently, the time step must be at least two to three orders of magnitude smaller than the grid spacing. For the indicated spatial resolution,  $\Delta\xi \sim 10^{-2}$ , we found it was necessary to take  $\Delta\tau \sim 10^{-7}$  to ensure numerical stability.

Figure 2 shows the evolution of  $|u(\xi, \tau)|$  with the Gaussian initial condition,  $A_0 = 3$  and  $L(0) = 0.2$ . The rescaled wave  $u(\xi, \tau)$  separates into three pieces. The middle one stays in the center of the domain while the other two waves move away from the origin on each side. Figure 3 shows that  $\max_\xi |u(\xi, \tau)|$  slightly decreases with  $\tau$ . Due to our choice of the rescaling factor,  $\|u_\xi(\cdot, \tau)\|_{L^2}$  is constant. We also

observe that  $\|u_{\xi\xi}(\cdot, \tau)\|_{L^2}$  remains bounded. Returning to the primitive variables, the maximum integration time  $\tau = 6$  corresponds to  $t = 0.0098$ ,  $\|\psi_x\|_{L^2} = 334.58$  and  $\|\psi_{xx}\|_{L^2} = 1.56 \times 10^6$ . For the Lorentzian initial condition (2.10) with  $A_0 = 3$  and  $L(0) = 1$ , the maximum integration time  $\tau = 0.16$  corresponds to  $t = 0.008$ ,  $\|\psi_x\|_{L^2} = 109.8$  and  $\|\psi_{xx}\|_{L^2} = 1.17 \times 10^5$ .

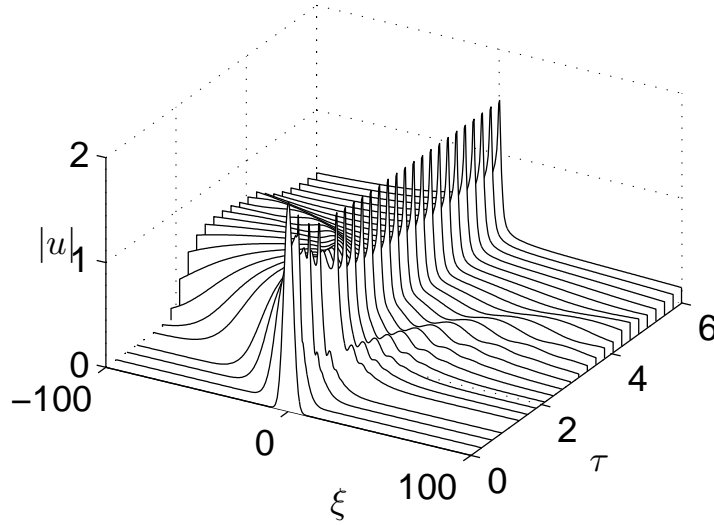


FIGURE 2.  $|u|$  versus  $\xi$  and  $\tau$ , for initial condition (2.9) with  $A_0 = 3$ , and nonlinearity  $\sigma = 2$ .

For a detailed description of singularity formation, we turn to the evolution of the parameters  $a$  and  $b$  as functions of  $\tau$ . For both families of initial conditions (2.9) and (2.10) and amplitudes  $A_0 = 2, 3, 4$ , we observe that  $a$  and  $b$  tend to constants  $A$  and  $B$  as  $\tau$  gets large. Figures 4 and 5 respectively display  $a$  and  $b$  versus  $\tau$  for initial conditions (2.9) and (2.10) and  $A_0 = 3$ .

Turning to the limiting profile of the solution, we write  $u$  in terms of amplitude and phase in the form  $u \equiv |u|e^{i\phi(\xi, \tau)}$ , Figure 6 shows that  $|u|$  tends to a fixed profile as  $\tau$  increases. Moreover, as shown in Figure 7, the phase at the origin is linear for  $\tau$  large enough, namely  $\phi(0, \tau) \sim C\tau$ . The constant  $C$  is obtained by fitting the phase at the origin using linear least squares over the interval  $[\tau_{max}/2, \tau_{max}]$ . After extracting this linear phase, the rescaled solution  $u$  tends to a time-independent function, (Figure 8):

$$(2.11) \quad u(\xi, \tau) \sim S(\xi)e^{i(\theta+C\tau)} \quad \text{as } \tau \rightarrow \infty.$$

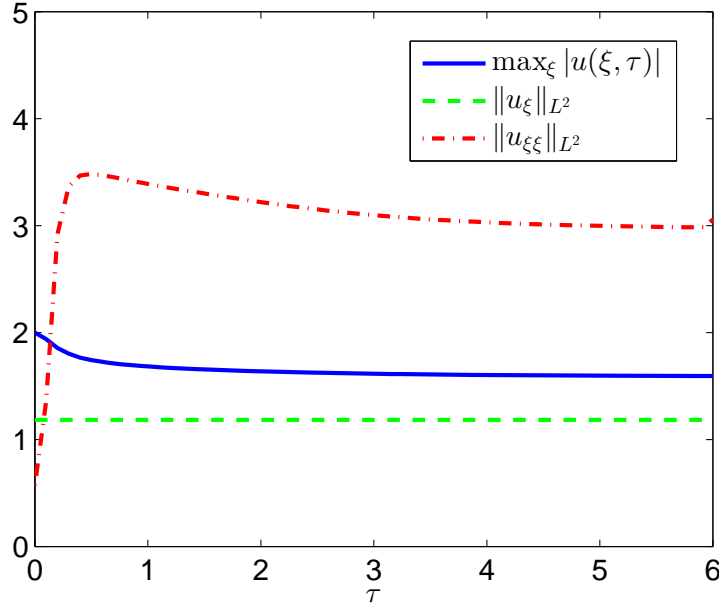


FIGURE 3.  $\max_{\xi} |u(\xi, \tau)|$ ,  $\|u_{\xi}(\cdot, \tau)\|_{L^2}$ , and  $\|u_{\xi\xi}(\cdot, \tau)\|_{L^2}$  versus  $\tau$ , same initial conditions as in Fig. (2).

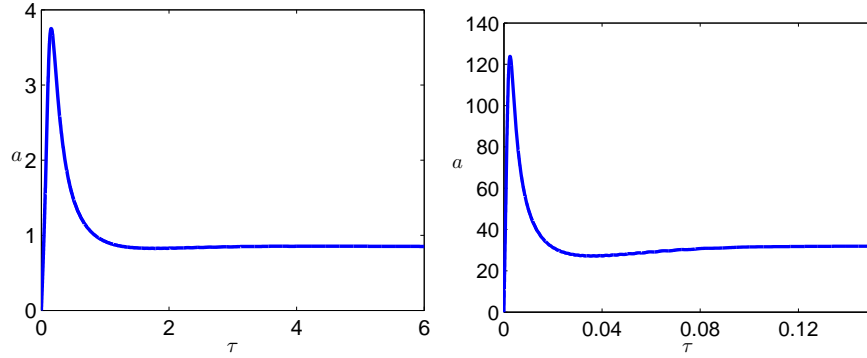


FIGURE 4. Time evolution of  $a(\tau)$ , with initial condition (2.9) (left) and (2.10) (right),  $A_0 = 3$ .

To check the accuracy of our computation, we compute the scaling factor  $L(t)$  in different ways. Either from the invariant quantities (2.8)

$$(2.12) \quad L_e = \left( \frac{E(\psi)}{E(u)} \right)^{-\frac{\sigma}{1+\sigma}}, \quad L_m = \left( \frac{M(\psi)}{M(u)} \right)^{-\frac{\sigma}{1-\sigma}}$$

or from integration of (2.3a),

$$(2.13) \quad L_a = e^{-\int_0^{\tau} a(\tau) d\tau}.$$



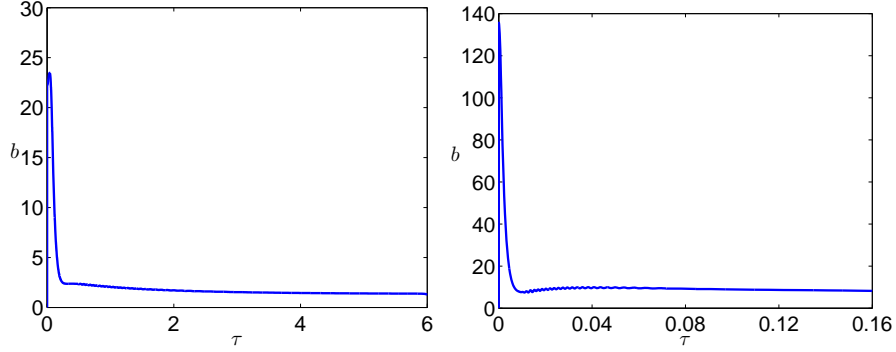


FIGURE 5. Time evolution of  $b(\tau)$ , with initial condition (2.9) (left) and (2.10) (right),  $A_0 = 3$ .

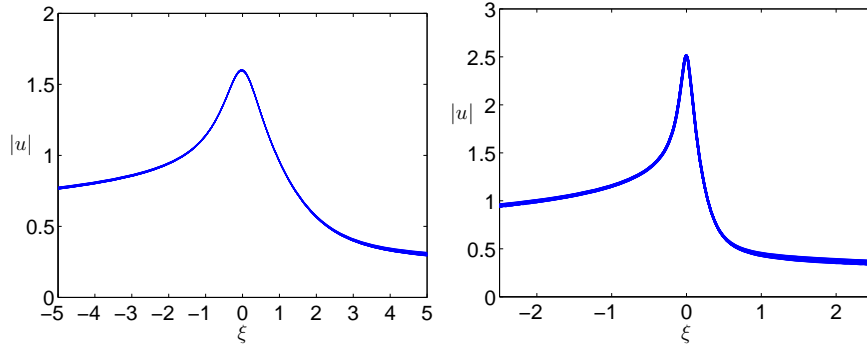


FIGURE 6.  $|u(\xi, \tau)|$  versus  $\xi$ , with initial condition (2.9) for  $\tau$  from 4.05 to 6 with an increment of 0.08. (left) and initial condition (2.10) for  $\tau$  from 0.12 to 0.16 with an increment of 0.002. (right).

Since we have real initial conditions, we cannot use the momentum. Table 1 shows the values of  $L(t)$  obtained in the simulation corresponding to the initial condition  $\psi_0(x) = 3e^{-2x^2}$  and  $\sigma = 2$ . The results are in good agreement.

TABLE 1. Estimates of  $L(\tau)$ , calculated using (2.12) and (2.13), with the initial condition (2.9),  $A_0 = 3$ .

$\tau$	1	2	3	4	5	6
$L_e$	0.03545	0.015233	0.006588	0.002811	0.001196	0.000595
$L_m$	0.03545	0.015233	0.006588	0.002811	0.001196	0.000555
$L_a$	0.035449	0.015233	0.006588	0.002811	0.001196	0.000555

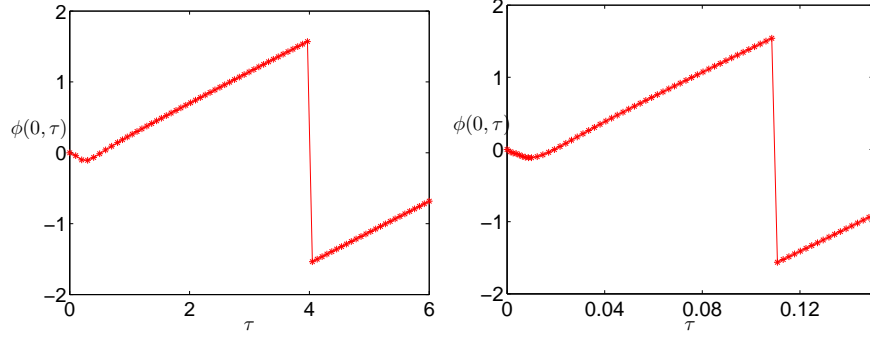


FIGURE 7. Time evolution of the phase at the origin  $\phi(0, \tau)$ , with initial conditions (2.9) (left) and (2.10) (right).

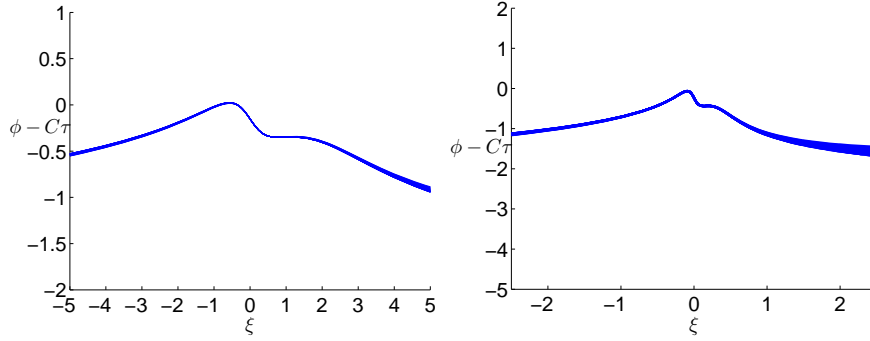


FIGURE 8. Time evolution of the modified phase  $\phi(\xi, \tau) - \phi(0, \tau)$ , with initial conditions (2.9) for  $\tau$  from 4.05 to 6 with an increment of 0.08. (left) and (2.10) for  $\tau$  from 0.12 to 0.16 with an increment of 0.002. (right).

Using (2.3) and the fact  $a(\tau)$  and  $b(\tau)$  tend to constants  $A$  and  $B$ , we conclude

$$(2.14) \quad L^2 \sim 2A(t^* - t),$$

and,

$$(2.15) \quad \frac{dx_0}{dt} = \frac{B}{\sqrt{2A(t^* - t)}},$$

where  $t^*$  is the blowup time. It follows

$$x_0 \sim x^* - B\sqrt{2(t^* - t)/A},$$

where  $x^*$  is the position of  $\max_x |\psi(x, t^*)|$ . Substituting into (2.7), we obtain

$$(2.16) \quad S_{\xi\xi} - CS + iA(\frac{1}{4}S + \xi S_\xi) - iBS_\xi + i|S|^4 S_\xi = 0.$$

Introducing the scaling

$$(2.17) \quad \tilde{\xi} = \sqrt{C}\xi, \quad Q(\tilde{\xi}) = C^{-\frac{1}{8}}S(\xi),$$

and dropping the tildes, we have

$$Q_{\xi\xi} - Q + i\alpha(\frac{1}{4}Q + \xi Q_\xi) - i\beta Q_\xi + i|Q|^4 Q_\xi = 0,$$

with the rescaled constants:

$$(2.18) \quad \alpha \equiv \frac{A}{C}, \quad \beta \equiv \frac{B}{\sqrt{C}}$$

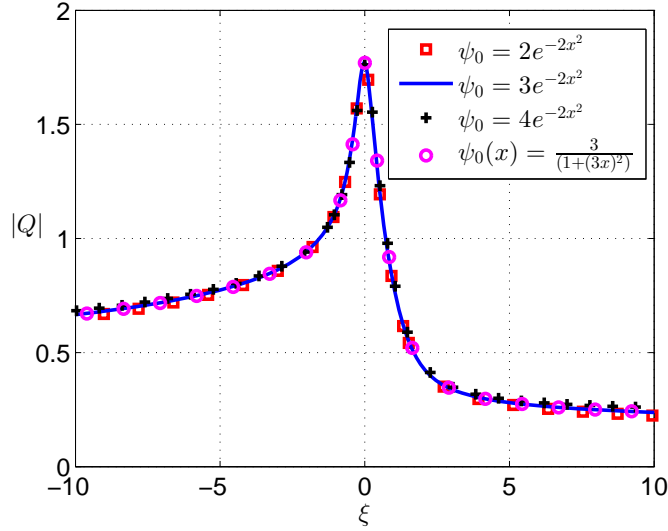
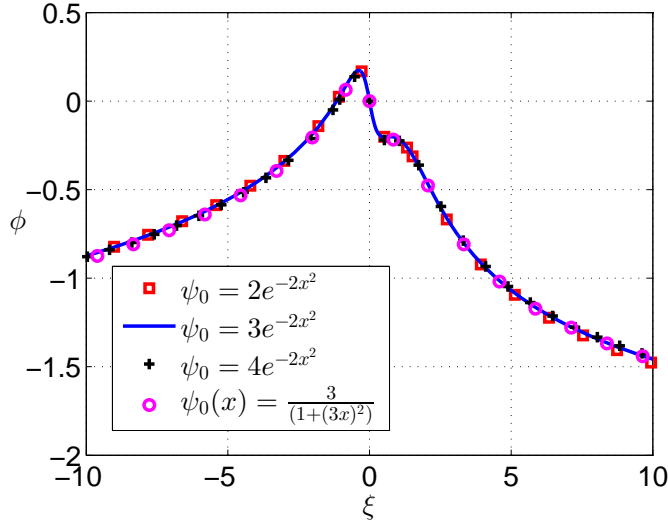
Like supercritical NLS, we find that the coefficients  $\alpha$  and  $\beta$  and the function  $Q$  are independent of the initial conditions. Table 2 shows that the ratios  $\alpha$  and  $\beta$  take the values  $\alpha \sim 1.95$  and  $\beta \sim 2.2$ . In Figure 9 and 10, we see that the amplitudes and the phase of the function  $Q$  constructed from the different initial conditions are coincide.

TABLE 2. Limiting values of the parameters for various initial conditions.

$u_0$	$C$	$A$	$B$	$\alpha$	$\beta$
$2e^{-2x^2}$	1.594	3.159	2.866	1.98	2.27
$3e^{-2x^2}$	0.435	0.854	1.5	1.96	2.25
$4e^{-2x^2}$	0.098	0.187	0.691	1.91	2.21
$\frac{3}{(1+(3x)^2)}$	16.35	31.82	8.965	1.94	2.22

In conclusion, we have observed that for a large class of initial conditions, solutions to (1.7) with quintic nonlinearity ( $\sigma = 2$ ) may blow up in a finite time. Their local description near the singularity point is, up to a rescaling, given by (1.12).

The inclusion of the translation parameter is a significant difference from NLS with power law nonlinearity. While later studies on singularity formation in NLS allowed for symmetry breaking [11], the preservation of radial symmetry under the flow strongly simplifies both the computations and the analysis. Due to the mixture of hyperbolic and dispersive terms in gDNLS, no such symmetry preservation is available, and we must be wary of the tendency for the solution to migrate rightwards.

FIGURE 9. Asymptotic profile  $|Q(\xi)|$  for different initial data.FIGURE 10. Asymptotic phase  $\phi(\xi) \equiv \arg(Q(\xi))$  for different initial data.

### 3. gDNLS WITH OTHER POWER NONLINEARITIES

The following calculations address the question of singularity for solutions of (1.7) when the power in the nonlinear term  $|\psi|^{2\sigma}\psi_x$  is such that  $1 < \sigma < 2$ . We recall that  $\sigma = 1$  corresponds to the usual DNLS equation which is  $L^2$ -critical. Our calculations cover the values of  $\sigma$

down to 1.1. Computational difficulties precluded us from reducing it much further.

Figure 11 shows that  $a(\tau)$  and  $b(\tau)$  tend to constant values as  $\tau$  increases. For convenience, we have plotted  $a(\tau)/a_M$  and  $b(\tau)/b_M$  versus  $\tau/\tau_M$ , where  $\tau_M$  is the maximum time of integration and  $a_M = a(\tau_M)$ ,  $b_M = b(\tau_M)$ . The initial condition is  $\psi_0(x) = 3e^{-2x^2}$  when  $\sigma = 1.7, 1.5$  and  $1.3$ , while  $\psi_0 = 4e^{-2x^2}$  for  $\sigma = 1.1$ . We also remark that the more supercritical, the larger  $\sigma$  is, the shorter the transient period. Table 3 shows that  $\alpha$  decreases as  $\sigma$  varies from 2 to 1.1, while  $\beta$  first decreases and then increases.

The main conclusion of our study is that for this range of values of  $\sigma$ , solutions to (1.7) may blow up in a finite time and their local structure is similar to that of the case  $\sigma = 2$  discussed in the previous section and is given by (1.12).

TABLE 3. Values of  $\alpha$  and  $\beta$  as  $\sigma$  approaches to 1.

$\sigma$	2	1.7	1.5	1.3	1.1
$\alpha$	1.98	1.26	0.85	0.38	0.04
$\beta$	2.27	2.11	1.68	1.63	1.90

#### 4. BLOWUP PROFILE

This section is devoted to the study of the nonlinear elliptic equation (1.13) satisfied by the complex profile function  $Q$ . It is helpful to change variables, letting  $\eta = \xi - \frac{\beta}{\alpha}$ , leading to

$$(4.1) \quad Q_{\eta\eta} - Q + i\alpha\left(\frac{1}{2\sigma}Q + \eta Q_\eta\right) + i|Q|^{2\sigma}Q_\eta = 0.$$

We seek profiles  $|Q(\eta)|$  that decrease monotonically with  $|\eta|$ , satisfying the conditions

$$Q(\eta) \rightarrow 0 \quad \text{as} \quad \eta \rightarrow \pm\infty.$$

This can be viewed as a nonlinear eigenvalue problem, with eigenparameter  $\alpha$ , and eigenfunction  $Q$ . As the equation is invariant to multiplication by a constant phase, we can assume, in addition, that  $Q(0)$  is real (for example).

##### 4.1. Properties of the Asymptotic Profile.

**Proposition 4.1.** *The asymptotic behavior of solutions to (4.1) as  $\eta \rightarrow \pm\infty$ , is given by  $Q = c_1^\pm Q_1 + c_2^\pm Q_2$  where*

$$(4.2) \quad Q_1 \approx |\eta|^{-\frac{i}{\alpha} - \frac{1}{2\sigma}}, \quad Q_2 \approx e^{i(-\frac{\sigma}{2}\eta^2)} |\eta|^{\frac{i}{\alpha} + \frac{1}{2\sigma} - 1},$$

and  $c_1^\pm, c_2^\pm$  are complex numbers.

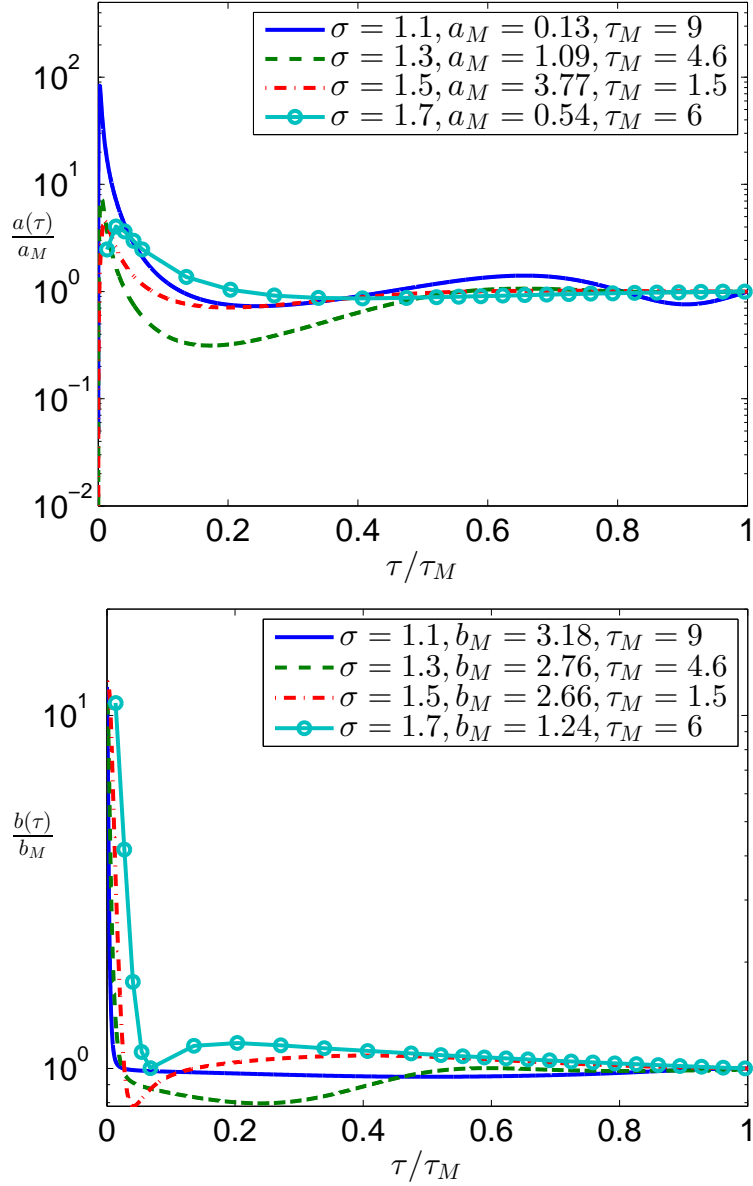


FIGURE 11.  $a(\tau)$  (up) and  $b(\tau)$  (down) versus  $\tau$ , after normalization by  $a_M = a(\tau_M)$  and  $b_M = b(\tau_M)$ ,  $\tau_M = \max(\tau)$ .

*Proof.* We first write  $Q(\eta) = X(\eta)Z(\eta)$  and choose  $X$  so that the resulting second-order equation for  $Z$  does not contain first order terms.

After substitution in the  $Q$ -equation, we get

$$(4.3) \quad \begin{aligned} & XZ_{\eta\eta} + (2X_\eta + i\alpha\eta X + iX|X|^{2\sigma}|Z|^{2\sigma})Z_\eta \\ & + (X_{\eta\eta} - X + i\frac{\alpha}{2\sigma}X + i\alpha\eta X_\eta + i|X|^{2\sigma}|Z|^{2\sigma}X_\eta)Z = 0. \end{aligned}$$

We now let

$$(4.4) \quad \begin{aligned} X &= \exp \left\{ -i\frac{\alpha}{4}\eta^2 - i\frac{1}{2} \int_0^\eta |Z|^{2\sigma} d\eta \right\} \\ &= \exp \left\{ -i\frac{\alpha}{4}\eta^2 - i\frac{1}{2} \int_0^\eta |Q|^{2\sigma} d\eta \right\}, \end{aligned}$$

so that the equation for  $Z$  reduces to

$$(4.5) \quad Z_{\eta\eta} + \left( \frac{i\alpha(1-\sigma)}{2\sigma} - 1 + \frac{(\alpha\eta)^2}{4} + \frac{|Z|^{4\sigma}}{4} + \frac{\alpha}{2}\eta|Z|^{2\sigma} - \frac{i}{2}(|Z|^{2\sigma})_\eta \right) Z = 0.$$

Denoting  $Z = Ae^{i\varphi}$  and  $\theta = \varphi_\eta$ , we rewrite (4.5) in terms of phase and amplitude:

$$(4.6a) \quad \frac{A''}{A} - \theta^2 - 1 + \frac{\alpha^2\eta^2}{4} + \frac{\alpha\eta}{2}A^{2\sigma} + \frac{1}{4}A^{4\sigma} = 0$$

$$(4.6b) \quad \theta' + 2\theta\frac{A'}{A} + \frac{\alpha(1-\sigma)}{2\sigma} - \frac{1}{2}(A^{2\sigma})' = 0$$

Anticipating that  $A \rightarrow 0$  when  $\eta \rightarrow \pm\infty$ , we see that to balance the quadratic and constant in  $\eta$  terms of (4.6a), we must have

$$(4.7) \quad \theta_1 = \left( \frac{\alpha\eta}{2} - \frac{1}{\alpha\eta} \right) + \gamma_1(\eta), \quad \theta_2 = - \left( \frac{\alpha\eta}{2} - \frac{1}{\alpha\eta} \right) + \gamma_2(\eta)$$

where  $\gamma_{1,2}(\eta)$  is at most  $O(\eta^{-1})$ . This leads to two cases:

**Case 1.**  $\theta_1 = (\frac{\alpha\eta}{2} - \frac{1}{\alpha\eta}) + \gamma_1(\eta)$ . Assuming  $A_1 \approx c_1^\pm |\eta|^{-p}$ , where  $c_1$  is a constant, we get from (4.6b) that  $p = 1/2\sigma$  by balancing the  $O(1)$  terms.

Substituting these estimates of  $\theta_1$  and  $A_1$  into (4.6a), we have to balance the  $O(1)$  terms  $\alpha\eta\gamma_1$  and  $\frac{\alpha}{2}\eta A_1^{2\sigma}$ . Hence, as  $\eta \rightarrow \pm\infty$ ,

$$(4.8) \quad \theta_1 \approx \frac{\alpha\eta}{2} - \frac{1}{\alpha\eta} + \frac{1}{2}|Q_1|^{2\sigma} + o(\eta^{-1}); \quad A_1 \approx c_1^\pm |\eta|^{-1/2\sigma} (1 + o(1)).$$

Retaining  $\gamma_1$  is essential since it is of order  $O(\eta^{-1})$  and is the only term capable of balancing  $\eta A_1^{2\sigma}$ . Returning to the function  $Q_1$ , we get one family of solutions with the farfield behavior

$$(4.9) \quad Q_1 \approx c_1^\pm |\eta|^{-\frac{1}{2\sigma} - \frac{i}{\alpha}} \text{ as } \eta \rightarrow \pm\infty.$$

**Case 2.**  $\theta_2 = -(\frac{\alpha\eta}{2} - \frac{1}{\alpha\eta}) + \gamma_2(\eta)$ . Assuming, again,  $A_2$  is asymptotically a power law, we get from (4.6b),  $A_2 \approx c_2^\pm |\eta|^{-1+\frac{1}{2\sigma}}$ , where  $c_2^\pm$  is a constant.

Substituting back into (4.6a) we get  $\gamma_2 \approx -\frac{1}{2} |A_2|^{2\sigma}$ , so that

$$(4.10) \quad \theta_2 \approx -\frac{\alpha\eta}{2} + \frac{1}{\alpha\eta} - \frac{1}{2} |Q_2|^{2\sigma} + o(\eta^{1-2\sigma}); \quad A_2 \approx c_2^\pm |\eta|^{-1+\frac{1}{2\sigma}} (1 + o(1))$$

leading to

$$(4.11) \quad Q_2 \approx c_2^\pm e^{-i\frac{\alpha}{2}\eta^2} |\eta|^{\frac{i}{\alpha} + \frac{1}{2\sigma} - 1} e^{-i \int_0^\eta |Q_2|^{2\sigma} d\eta}.$$

Finally, we can neglect the last term in the phase and write

$$(4.12) \quad Q_2 \approx c_2^\pm e^{-i\frac{\alpha}{2}\eta^2} |\eta|^{\frac{i}{\alpha} + \frac{1}{2\sigma} - 1} \text{ as } \eta \rightarrow \pm\infty.$$

□

**Proposition 4.2.** *If  $Q$  is a solution of (4.1) with  $Q_\eta \in L^2(\mathbb{R})$  and  $Q \in L^{4\sigma+2}(\mathbb{R})$ , its energy vanishes:*

$$(4.13) \quad \int_{-\infty}^{\infty} |Q_\eta|^2 d\eta + \frac{1}{(\sigma+1)} \Im \int_{-\infty}^{\infty} |Q|^{2\sigma} \bar{Q} Q_\eta d\eta = 0.$$

*Proof.* Multiplying (4.1) by  $\bar{Q}_\eta$ , taking the imaginary parts, and integrating over the whole line gives

$$(4.14) \quad \alpha \Re \int \left( \frac{Q}{2\sigma} + \eta Q_\eta \right) \bar{Q}_\eta d\eta + \Re \int |Q|^{2\sigma} Q_\eta \bar{Q}_\eta d\eta = 0.$$

The first integral of (4.14) can be written

$$(4.15) \quad \alpha \Re \int \left( \frac{Q}{2\sigma} + \eta Q_\eta \right) \bar{Q}_\eta d\eta = \left( -\frac{\sigma+1}{2\sigma} \right) \alpha \int |Q_\eta|^2 d\eta.$$

Using (4.1) to express  $\bar{Q}_\eta$ , the second integral becomes

$$(4.16) \quad \begin{aligned} & \Re \int |Q|^{2\sigma} Q_\eta \left( \bar{Q} + i\alpha \left( \frac{1}{2\sigma} \bar{Q} + \eta \bar{Q}_\eta \right) \right) |Q|^{2\sigma} \bar{Q}_\eta d\eta \\ &= \Re \int |Q|^{2\sigma} Q_\eta \bar{Q} + \frac{i\alpha}{2\sigma} |Q|^{2\sigma} Q_\eta \bar{Q} d\eta \\ &= -\frac{\alpha}{2\sigma} \Im \int |Q|^{2\sigma} Q_\eta \bar{Q} d\eta. \end{aligned}$$

Combining (4.15) and (4.16), we obtain (4.13). □

**Proposition 4.3.** *If  $Q$  is a solution of (4.1) with  $\sigma > 1$  and  $\alpha > 0$ , and  $Q \in H^1(\mathbb{R}) \cap L^{2\sigma+2}(\mathbb{R})$ , then  $Q \equiv 0$ .*



*Proof.* Multiplying (4.1) by  $\bar{Q}$ , taking the imaginary part, and integrating over  $\mathbb{R}$ , we get

$$(4.17) \quad \frac{\alpha}{2} \left( \frac{1}{\sigma} - 1 \right) \int |Q|^2 d\eta = 0,$$

thus  $Q$  has to be identically zero. □

Consequently, solutions with finite energy have an infinite  $L^2$ -norm.

#### 4.2. Numerical Integration of the Boundary Value Problem.

The purpose of this section is the numerical integration of the BVP (4.1) in order to better understand the asymptotic profile of the singular solutions of gDNLS. We look for solutions that behave like  $c_1^\pm Q_1$  as  $|\eta| \rightarrow \infty$ , where  $c_1^\pm$  are complex constants, because  $Q_2$  does not have finite energy. It is convenient to rewrite the large  $\eta$  behavior as a Robin boundary condition of the form

$$(4.18) \quad -Q + i\alpha \left( \frac{1}{2\sigma} Q + \eta Q_\eta \right) = 0, \quad |\eta| \rightarrow \infty.$$

Solutions of (4.1) depend on the coefficient  $\alpha$ . Since the equation is invariant under phase translation, we need an additional condition; for example, setting the phase to zero at a particular point is satisfactory. This suggests that  $\alpha$  needs to take particular values, like in the supercritical NLS problem, [21]. We are particularly interested in the character of the asymptotic profile and of the coefficient  $\alpha$  as  $\sigma$  approaches the critical case  $\sigma = 1$ . Our basic approach is a continuation method in the parameter  $\sigma$ .

At first, we attempted to integrate (4.1) with boundary conditions (4.18) for values of  $\sigma$  starting from  $\sigma = 2$  to about  $\sigma = 1.2$ . We observed that the peak of  $|Q|$  rapidly moved to the left of the domain as  $\sigma$  decreased, limiting our calculations, (Figure 12).

To reach values of  $\sigma$  closer to 1, we returned to (1.13) (which is equivalent to (4.1) after the translation  $\xi = \eta + \beta/\alpha$ ). Now the parameter  $\beta$  is free and will be chosen so that the maximum of  $|Q|$  is at  $\xi = 0$ . This adds a condition, namely  $|Q|_\xi(0) = 0$  and an additional unknown, the coefficient  $\beta$ . Figure 13 shows that the solution of (1.13) when  $\sigma$  varies from 2 to 1.08. As  $\sigma \rightarrow 1$ , we make several observations on  $Q$ . The amplitude increases, and the left shoulder becomes lower. Oscillations also appear in the real and imaginary components (Figure 14). We observe that the parameter  $\alpha$  decreases as  $\sigma$  approaches 1, while  $\beta$  first decreases and then increases (Figure 15). A detailed analysis of the dependence of these parameters on  $\sigma$  is the subject of a future study.

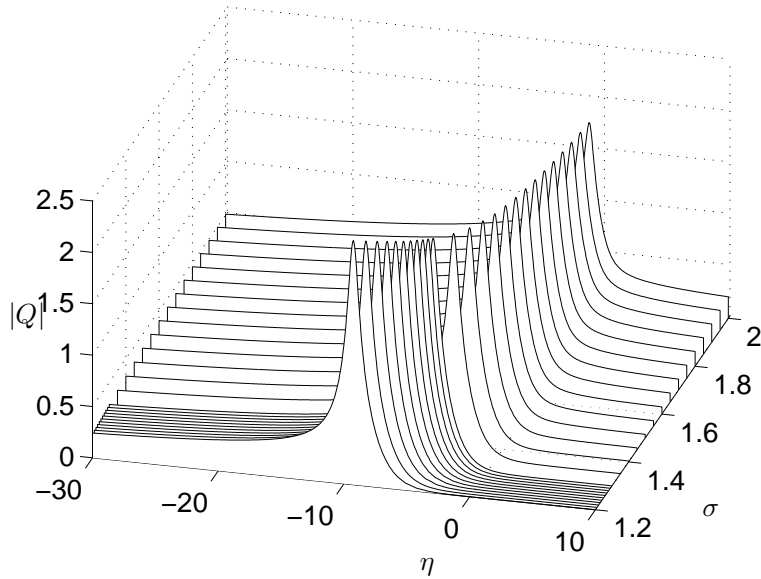


FIGURE 12. Asymptotic profile  $|Q(\eta)|$  for various  $\sigma$ , where  $\beta$  has been translated to zero and the peak is permitted move.

As a practical matter, we integrated (1.13) in two adjacent domains  $(-\infty, 0]$  and  $[0, \infty)$ , using the multipoint feature of the MATLAB `bvp4c` solver, with Robin boundary conditions at  $\pm\infty$  and continuity conditions on  $Q$  and its first derivative  $Q_\xi$  at  $\xi = 0$ . Additional details are given in Appendix A.

## 5. DISCUSSION

We have numerically solved a derivative NLS equation with a general power nonlinearity and found evidence of a finite time singularity. We have determined that there is a square root blowup rate for the scaling factor  $L(t)$ . This implies that Sobolev norms should grow as

$$\|\partial_x^s \psi(x, t)\|_{L^2} \sim (t^* - t)^{\frac{\sigma-1}{4\sigma} - \frac{s}{2}}.$$

As with supercritical NLS, this equation has a universal blowup profile of the form (1.12). Indeed,  $Q$ ,  $\alpha$  and  $\beta$  are solutions of a nonlinear eigenvalue problem, and they do not depend on the initial conditions. They depend on the power nonlinearity  $\sigma$ . Another similarity to supercritical NLS is that the blowup profile,  $Q$ , is not in  $L^2$  and has zero energy. Note that there are other types of singular solutions to supercritical NLS that were found recently [4] [7].

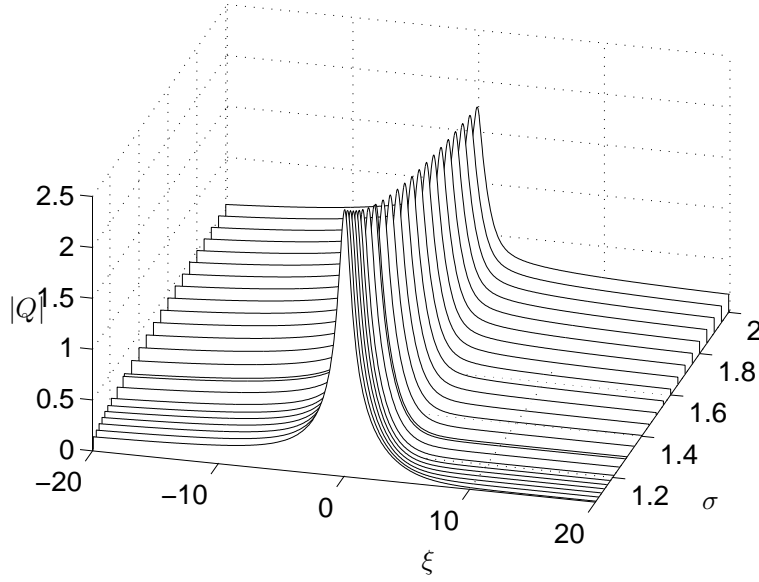


FIGURE 13. Asymptotic profile  $|Q(\xi)|$  for various  $\sigma$ , where  $\beta$  is a free parameter and the peak is fixed at the origin.

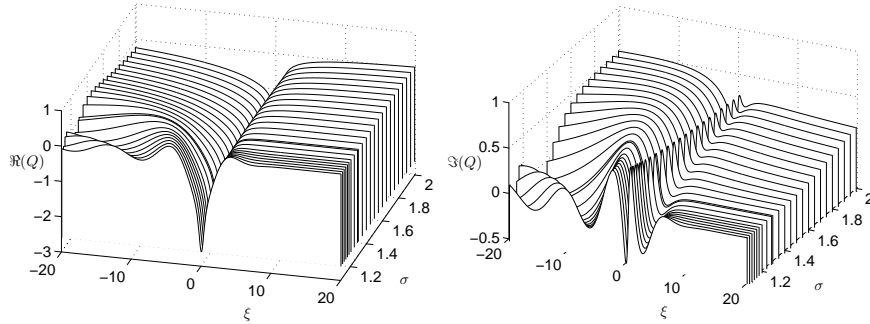


FIGURE 14. Asymptotic profile  $\Re(Q)$  (left) and  $\Im(Q)$  (right) for various  $\sigma$ .

To conclude, we present numerical simulations of the DNLS equation with  $\sigma = 1$  and several Gaussian initial conditions ( $A_0 = 3, 4, 5, 6$ ). In all our simulations, the solution separates into several waves and disperses. None of our simulations have shown any evidence of a finite time singularity, although the transient dynamics can be quite violent. Figure 16 shows the evolution of  $|\psi(x, t)|$  with the Gaussian initial condition:  $\psi_0(x) = 6e^{-2x^2}$ . The maximum value of  $|\psi|$  increases slowly in time and then stabilizes. We also integrated DNLS using the dynamic

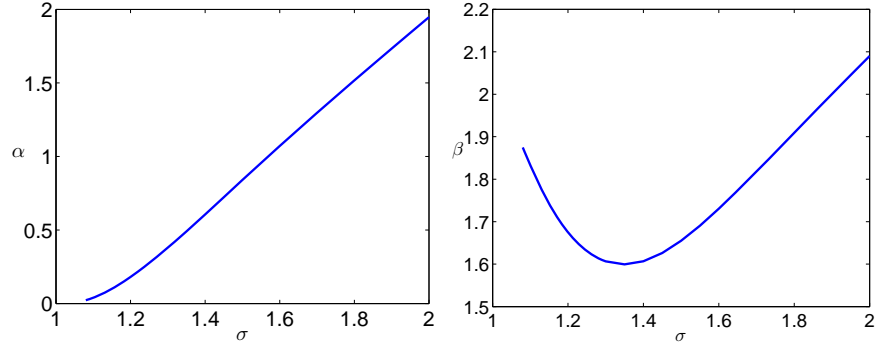


FIGURE 15. Coefficients  $\alpha$  (left) and  $\beta$  (right) versus  $\sigma$ .

rescaling method. We found that  $a(\tau)$  rapidly tends to zero and that the scaling factor  $L(t)$  has a lower bound away from zero, (Figure 17). This is different with the critical NLS, which has a blowup rate at  $\{\ln \ln[(t^* - t)^{-1}]/(t^* - t)\}^{1/2}$ , due to the slow decay rate of  $a(\tau)$ , [12].

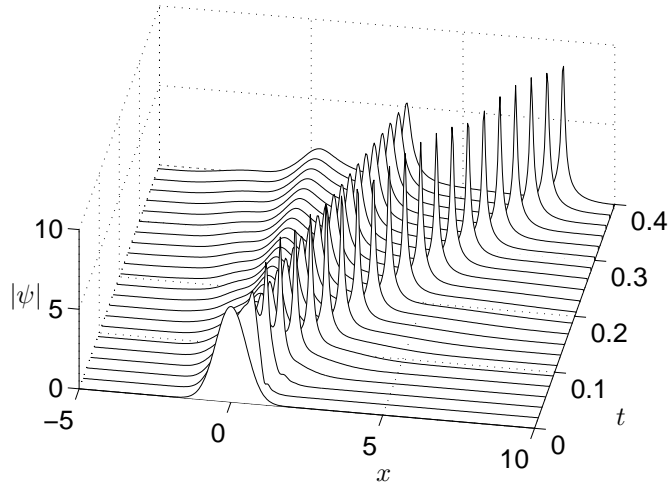


FIGURE 16. Time evolution of  $|\psi(x, t)|$  for  $\sigma = 1$ .

#### APPENDIX A. NUMERICAL SOLUTION OF THE BOUNDARY VALUE PROBLEM

To integrate the nonlinear elliptic equation (1.13) for  $Q$ , we rewrite as a first order system for the four unknowns,  $\Re(Q)$ ,  $\Im(Q)$ ,  $\Re(Q_\xi)$  and  $\Im(Q_\xi)$ . As discussed before, we solve the system in two adjacent domains  $[-A_L, 0]$  and  $[0, A_R]$ . The solutions and their first order derivatives are matched by continuity at  $\xi = 0$ , while the boundary conditions

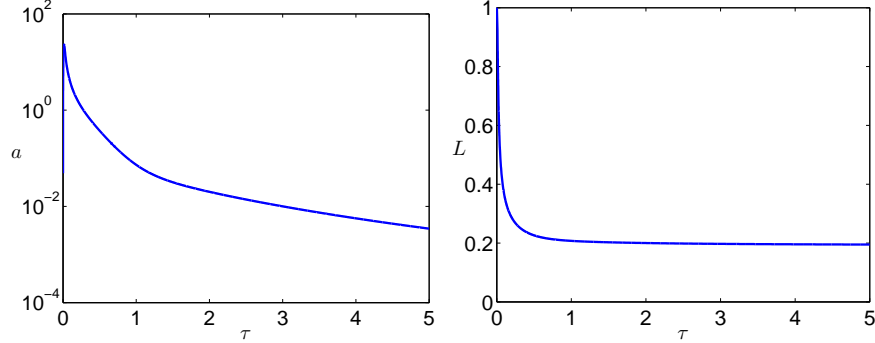


FIGURE 17. Time evolution of  $a$  (Left) and  $L$  (Right) for  $\sigma = 1$ .

at infinity are of Robin type. We denote

$$y_1^\pm = \Re(Q), \quad y_2^\pm = \Im(Q), \quad y_3^\pm = \Re(Q_\xi), \quad y_4^\pm = \Im(Q_\xi),$$

where  $y^-$  and  $y^+$  are the solutions in  $[-A_L, 0]$  and  $[0, A_R]$  respectively. The system takes the form:

$$(A.1) \quad \begin{aligned} \frac{dy_1^\pm}{d\xi} &= y_3^\pm, \\ \frac{dy_2^\pm}{d\xi} &= y_4^\pm, \\ \frac{dy_3^\pm}{d\xi} &= y_1^\pm + \alpha\left(\frac{1}{2\sigma}y_2^\pm + \xi y_4^\pm\right) - \beta y_4^\pm + [(y_1^\pm)^2 + (y_2^\pm)^2]^\sigma y_4^\pm, \\ \frac{dy_4^\pm}{d\xi} &= y_2^\pm - \alpha\left(\frac{1}{2\sigma}y_1^\pm + \xi y_3^\pm\right) - \beta y_3^\pm - [(y_1^\pm)^2 + (y_2^\pm)^2]^\sigma y_3^\pm. \end{aligned}$$

Solving four first order ODEs in two regions with two unknown parameters requires imposing ten boundary conditions. Four of them are the Robin boundary condition (4.18) relating  $\Re(Q)$ ,  $\Im(Q)$ ,  $\Re(Q_\xi)$  and  $\Im(Q_\xi)$  at  $\xi = -A_L$  and  $\xi = A_R$  respectively:

$$(A.2) \quad \begin{aligned} -y_1^- - \frac{\alpha}{2\sigma}y_2^- - \alpha\xi y_4^- &= 0 \text{ at } \xi = -A_L, \\ -y_2^- + \frac{\alpha}{2\sigma}y_1^- + \alpha\xi y_3^- &= 0 \text{ at } \xi = -A_L, \\ -y_1^+ - \frac{\alpha}{2\sigma}y_2^+ - \alpha\xi y_4^+ &= 0 \text{ at } \xi = A_R, \\ -y_2^+ + \frac{\alpha}{2\sigma}y_1^+ + \alpha\xi y_3^+ &= 0 \text{ at } \xi = A_R. \end{aligned}$$

We impose the continuity of the solution at  $\xi = 0$ :

$$(A.3) \quad \begin{aligned} y_1^+(0) &= y_1^-(0), \\ y_2^+(0) &= y_2^-(0), \\ y_3^+(0) &= y_3^-(0), \\ y_4^+(0) &= y_4^-(0). \end{aligned}$$

The other two conditions are  $|Q(0)|_\xi = 0$  (the maximum value of  $Q$  is attained at the origin) and  $\Im(Q(0)) = 0$  (because the equation is invariant by phase translation) :

$$(A.4) \quad \begin{aligned} y_1^- y_3^- + y_2^- y_4^- &= 0 \text{ at } \xi = 0, \\ y_2^- &= 0 \text{ at } \xi = 0 \end{aligned}$$

We proceed using a continuation method with respect to  $\sigma$ , starting from  $\sigma = 2$  down to  $\sigma = 1.08$ . The MATLAB nonlinear solver `bvp4c` is used to integrate the system for each  $\sigma$ . The two domains are automatically handled using the multipoint feature, which permits for matching conditions at 0. One needs to provide a well-chosen initial guess. We use the final profile from our time-dependent simulation with the initial condition (2.9),  $A_0 = 3$  and  $\sigma = 2$ , in the domain  $[-10, 10]$  to extract the maximum bulk of the solution, (see Figures 9 and 10). This solution is then extended to a larger domain  $[-150, 50]$  with an increment of 10. As shown in Figure 14, more and more oscillations occur as  $\sigma$  approaches 1. The calculation becomes very delicate and we use smaller and smaller increments of  $\sigma$ , namely 0.05, 0.01 and 0.005 for  $\sigma$  in the intervals  $2 \geq \sigma \geq 1.3$ ,  $1.3 \geq \sigma \geq 1.2$  and  $1.2 \geq \sigma \geq 1.08$ , respectively. We set the maximum mesh points at  $5 \times 10^5$  and the tolerance of the difference between two iterations at  $10^{-6}$ .

## REFERENCES

- [1] Agrawal, G.P., *Nonlinear Fiber Optics*, Academic Press, San Diego, 2006.
- [2] Colliander, J., Keel, M., Staffilani, G., Takaoka, H., Tao, T., *A Refined Global Well-Posedness Result for Schrödinger Equations with Derivative*, SIAM J. Math. Anal., **34** (2002), 64–86.
- [3] DiFranco, J.C., Miller, P.D., *The semiclassical modified nonlinear Schrödinger equation I: Modulation theory and spectral analysis*, Physica D, **237** (2008), 947–997.
- [4] Fibich, G., Gavish, N., Wang, X.-P., *Singular ring solutions of critical and supercritical nonlinear Schrödinger equations*, Phys. D **231** (2007), 55–86.
- [5] Hao, C., *Well-Posedness for One-Dimensional Derivative Nonlinear Schrödinger Equations*, Commun. Pure Appl. Anal., **6** (2007), 997–1021.
- [6] Hayashi, N., Ozawa, T., *On the derivative nonlinear Schrödinger equation*. Physica D **55** (1992), 14–36.

- [7] Holmer, J., Roudenko, S., *On blow-up solutions to the 3D cubic nonlinear Schrödinger equation*, Appl. Math. Res. Express. AMRX 2007, no. 1, Art. ID abm004, 31 pp.
- [8] Kassam, A.K., Trefethen, L.N., *Fourth-Order Time-Stepping for Stiff PDEs*, SIAM J. Sci. Comput. **26** (2005), 1214–1233.
- [9] Kaup, D.J., Newell, A.C., *An exact solution for a derivative nonlinear Schrödinger equation*, J. Math. Phys., **19** (1978), 798–801.
- [10] Kenig, C.E., Ponce, G., Vega, L., *Smoothing effects and local existence theory for the generalized nonlinear Schrödinger equations*, Invent Math. **134** (1998), 489–545.
- [11] Landman, M.J., Papanicolaou, G.C., Sulem, C., Sulem, P.L., *Stability of isotropic singularities for the nonlinear Schrödinger equation*, Physica D. **47** (1991), 393–415.
- [12] Landman, M.J., Papanicolaou, G.C., Sulem, C., Sulem, P.L., *Rate of blowup for solutions of the nonlinear Schrödinger equation at critical dimension*, Physical Rev. A, **38**(8), (1988), 3837–3843.
- [13] Lee, J., *Global solvability of the derivative nonlinear Schrödinger equation*, Trans. Am. Math. Soc. **314** (1989), 107–118.
- [14] Linares, F., Ponce, G., *Introduction to Nonlinear Dispersive Equations*, Springer, Berlin (2009).
- [15] Liu, X., Simpson, G., Sulem, C., *Stability of Solitary Waves for a Generalized Derivative Nonlinear Schrödinger Equation*, arXiv:1206.3502, to appear in J. Nonlinear Science.
- [16] McLaughlin, D.W., Papanicolaou, G., Sulem, C., Sulem P.L., *The focusing singularity of the cubic Schrödinger equation*, Phys. Rev. A **34** (1986), 1200–1210.
- [17] Mjølhus, E., *On the modulational instability of hydromagnetic waves parallel to the magnetic field*, J. Plasma Phys., **16** (1976), 321–334.
- [18] Moses, J., Malomed, B., Wise, F., *Self-steepening of ultrashort optical pulses without self-phase-modulation*, Phys. Rev. A, **76** (2007), 1–4.
- [19] Passot, T., Sulem, P.L., *Multidimensional modulation of Alfvén waves*, Phys. Rev. E, **48** (1993), 2966–2974.
- [20] Shampine, L. F., *Singular boundary value problems for ODEs*, Appl. Math. Comput., **138** (2003), 99–112.
- [21] Sulem, C., Sulem, P.L., *The nonlinear Schrödinger equation: self-focusing and wave collapse*. Applied Mathematical Sciences, vol. 139, Springer, Berlin, 1999.
- [22] Tsutsumi, M., Fukuda, I., *On solutions of the derivative nonlinear Schrödinger equation, Existence and uniqueness theorem*, Funkcialaj Ekvacioj, **23** (1980), 259–277.

*E-mail address:* liuxiao@math.toronto.edu

DEPARTMENT OF MATHEMATICS, UNIVERSITY OF TORONTO, 40 ST. GEORGE ST., ROOM 6290, TORONTO, ONTARIO M5S 2E4, CANADA

*E-mail address:* gsimpson@umn.edu

SCHOOL OF MATHEMATICS, UNIVERSITY OF MINNESOTA, 206 CHURCH ST.  
SE, 127 VINCENT HALL, MINNEAPOLIS, MN 55455, USA

*E-mail address:* `sulem@math.toronto.edu`

DEPARTMENT OF MATHEMATICS, UNIVERSITY OF TORONTO, 40 ST. GEORGE  
ST., ROOM 6290, TORONTO, ONTARIO M5S 2E4, CANADA